Journal of Coordination Chemistry

ISSN: 0095-8972 (Print) 1029-0389 (Online) Journal homepage: http://www.tandfonline.com/loi/gcoo20

Copper(II) and nickel(II) complexes derived from a carbothioamide-5-pyrazolone ligand: synthesis, characterization, crystal structures, electrochemical, potentiometric and DNA-binding studies

Selma Akcha, Lamouri Hammal, Smail Triki, Luis Lezama, Bellara Nedjar-Kolli & Ouassini Benali Baitich

To cite this article: Selma Akcha, Lamouri Hammal, Smail Triki, Luis Lezama, Bellara Nedjar-Kolli & Ouassini Benali Baitich (2015) Copper(II) and nickel(II) complexes derived from a carbothioamide-5-pyrazolone ligand: synthesis, characterization, crystal structures, electrochemical, potentiometric and DNA-binding studies, Journal of Coordination Chemistry, 68:24, 4373-4394, DOI: 10.1080/00958972.2015.1096932

To link to this article: http://dx.doi.org/10.1080/00958972.2015.1096932

Accepted author version posted online: 22 Sep 2015.
Published online: 26 Oct 2015.

Journal of Coordination Chemistry, 2015
Vol. 68, No. 24, 4373–4394, http://dx.doi.org/10.1080/00958972.2015.1096932

Copper(II) and nickel(II) complexes derived from a carbothioamide-5-pyrazolone ligand: synthesis, characterization, crystal structures, electrochemical, potentiometric and DNA-binding studies

SELMA AKCHA†, LAMOURI HAMMAL‡, SMAIL TRIKI§, LUIS LEZAMA¶, BELLARA NEDJAR-KOLLI‡ and OUASSINI BENALI BAITICH*†

†Faculté de chimie, Laboratoire d'Hydrométallurgie et Chimie Inorganique Moléculaire, USTHB, Alger, Algeria
‡Faculté de chimie, Laboratoire de Chimie Organique Appliquée, USTHB, Alger, Algeria
§UMR CNRS 6521 – Université de Bretagne occidentale, Brest Cedex 3, France
¶Departamento de Química Inorgánica y BCMaterials, Universidad del País Vasco, Bilbao, Spain

(*Received 5 May 2015; accepted 2 September 2015*)

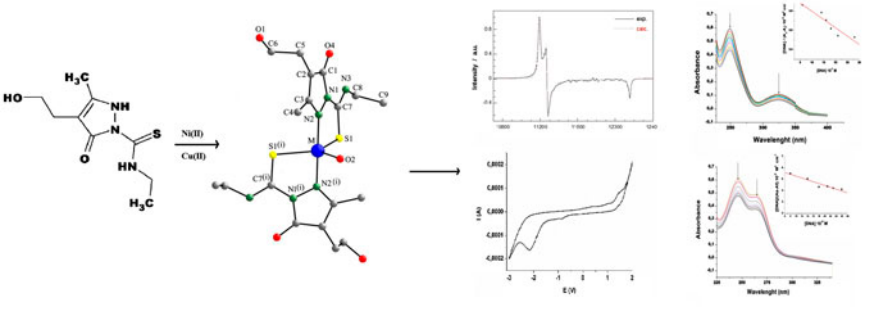

The synthesis of a 5-pyrazolone derivative (H_2L) bearing a carbothioamide group at N_1, N-ethyl-4-(2-hydroxyethyl)-3-methyl-5-oxo-2,5-dihydro-1H-pyrazole-1-carbothioamide, using a Keggin catalyst ($H_4SiW_{12}O_{14}{\cdot}nH_2O$), is described. Complexes of copper(II) and nickel(II) have been prepared with this potential ligand and studied by potentiometry. Processing the pH-metric titrations revealed remarkable chelation ability of the ligand and high stability constants for the complexes. The complexes have been characterized by IR, UV/visible, electrochemistry, magnetic measurements, Electron Paramagnetic Resonance (EPR) and single-crystal X-ray diffraction. The structures are $[Cu(HL)_2H_2O]{\cdot}2H_2O$ and $[Ni(HL)_2H_2O]{\cdot}2H_2O$, where the metal is five coordinate in an almost perfect trigonal bipyramidal geometry (D_{3h}). The pyrazolone derivative (H_2L) is a NS bidentate negative ligand, which coordinates to the metal through sulfur and amine nitrogen of the pyrazolone ring. The electronic results and the EPR of the complexes have been carefully studied in this (D_{3h}) crystal field with a special emphasis on the energy levels. DNA-binding experiments have been conducted by UV spectroscopy and electrochemistry. The results reveal an interaction between

*Corresponding author. Email: benali.baitich@gmail.com

the complexes and DNA and suggest an intercalative binding mode. UV titrations allowed determination of the binding constants K_b and revealed that the nickel(II) complex binds more strongly.

Keywords: Keggin catalyst; Pyrazolone; Copper(II); Nickel(II); Potentiometry; X-ray structure; Trigonal bipyramid; Electrochemistry; DNA

1. Introduction

Pyrazolone derivatives are of particular importance in pharmaceutical chemistry due to their numerous applications as analgesic [1], antipyretic [2], anti-inflammatory [3, 4], antibacterial [5], antifungal [6], antidepressant [7], and antitumor agents [8].

The substituted pyrazolone derivatives, following the example of the heterocyclic-substituted thioamides [9], have aroused considerable interest due to their chelating ability toward transition metal ions. The complexes of pyrazole-containing derivatives have been reported to possess antitumor activity comparable to that of cisplatin [10].

The most important methods for preparing this class of heterocycles are reactions between hydrazine derivatives with 1,3-diketones or their synthetic equivalents, known as the Knorr pyrazole synthesis [11]. Nevertheless, the use of heteropoly acids (HPAs), which are stronger acids than homogeneous acid catalysts, such as sulfuric acid or ion exchange resins, has now reached significant levels in different areas of organic chemistry, mainly because of the good yields and environmentally benign syntheses [12–15].

DNA is a key target for cancer chemotherapy; the first agents to be employed clinically in the treatment of human cancer are DNA cross-linking agents. Spectacular advances have occurred in recent years in the treatment of cancers, largely as the result of the development of better DNA-interactive agents [16]. For evaluating the anticancer activity of any newly synthesized complex, DNA binding is the predominant property looked for in pharmacology. The interaction between DNA and metal complexes is of paramount importance for understanding the mechanism [17].

This work describes a synthetic route to a 5-pyrazolone derivative H_2L, substituted by a carbothioamide moiety, an interesting potential ligand with several N, S, O donor sets.

A synthetic route for the synthesis of this ligand has been described in the literature and the X-ray structure elucidated [18]. In order to propose an effective synthesis, with a good yield and better environmental outcomes, a synthesis has been conducted using a Keggin catalyst ($H_4SiW_{12}O_{14}\cdot nH_2O$) (scheme 1). The reaction mechanism is suggested (scheme 2) and a comparison between such a route with the classical one is proposed. This ligand has been studied by IR, ^1H and ^{13}C NMR in order to investigate its dominant tautomeric form. A potentiometric study has been conducted in order to determine its acidobasic properties and its coordination ability.

Then, complexations with Cu(II) and Ni(II) are carried out and the resulting complexes characterized by cyclic voltammetry, IR, UV/visible, EPR, magnetic measurements, and single-crystal X-ray diffraction. DNA-binding experiments have been conducted on both complexes, by electronic spectrometry and electrochemistry, in order to investigate the binding mode and to calculate the binding constants.

2. Experimental

2.1. *Materials*

All chemicals were procured from Fluka and used without purification. Accurate concentrations of metal solutions were determined by titrations against EDTA. Fish Sperm DNA (FS-DNA) was kindly provided by the Department of Inorganic Chemistry of the University Rey Juan Carlos (Spain). Stock solution of FS-DNA (Sigma-Aldrich) was prepared by dissolving the sodium salt in buffer containing 15 mM of trisodium citrate and 150 mM of NaCl at pH 7.2. The solution was stirred for three days and kept at 4–5 °C for no longer than one week. The absorbance ratio of FS-DNA solution at λ_{max} 260 and 280 nm (A_{260}/A_{280}) was 2 : 1, which shows that FS-DNA was sufficiently free from protein contamination. The solution was standardized spectrophotometrically using its known molar absorbance coefficient at $\lambda = 260$ nm ($\varepsilon = 6600\ cm^{-1}\ M^{-1}$). Concentrated stock solutions of metal complexes were prepared by dissolving the required quantities in dimethyl sulfoxide (DMSO). The desired concentrations were achieved by dilutions in buffer (15 mM of trisodium citrate and 150 mM of NaCl at pH 7.2). Homogeneous solutions were obtained with DMSO content less than 1%.

2.2. *Syntheses*

2.2.1. Syntheses of the ligand H_2L. To a solution of **1** (10 mmol) and the appropriate isothiocyanates **2** was added 1% (1 µmol, 2×10^{-3} g) of Keggin catalyst ($H_4SiW_{12}O_{14}{\cdot}nH_2O$) in ethanol (schemes 1 and 2). The mixed solution was refluxed under magnetic stirring for 8 h. After cooling to room temperature, the white solid was collected by filtration and later recrystallized in ethanol. Yield: 80%.

In order to compare the yield obtained for the synthesis of **3** without using a heteropoly acid, the synthesis described in the literature has been carried out [18]. This procedure consists of refluxing furanone with ethylthiosemicarbazide in ethanol medium for 18 h. The obtained yield was 50%.

The HRESI mass spectrum of H_2L gave a quasi-molecular ion $(M + Na)^+$ peak at m/z = 252.0779.

^{1}H NMR (300 MHz, DMSO-d_6): 1.18 (t, J = 7 Hz, 3H, CH_3), 2.16 (s, 3H, CH_3); 2.34 (q, J = 7 Hz, 2H, CH_2), 2.39 (m, 3H, CH_2+OH), 3.60 (m, 2H, CH_2), 9.6 (br, NH), 11.15 (s, NH).

^{13}C NMR (75 MHz, DMSO-d_6): 13.17 (CH_3), 25.44 (CH_3), 59.54 (CH_2), 61.02 (CH_2), 66.67 (CH_2), 136.92 (C=C), 149.95 (C=C), 159.65 (C=O), 174.26 (C=S).

^{1}H NMR (300 MHz, $CDCl_3$): 1.33 (t, J = 6 Hz, 3H, CH_3), 2.23 (s, CH_3); 2.54 (t, J = 6 Hz, CH_2), 3.73 (m, CH_2), 3.80 (t, J = 6 Hz, CH_2), 9.7 (br, NH), 11.10 (s, NH).

The molecular structure of ligand can exist in two tautomeric forms, thione–thiol since it contains a thioamide NH–C=S functional group. Spectral data (^{1}H and ^{13}C NMR) reveal that in solution the favored tautomeric form in both DMSO and chloroform is the thione.

In addition to the spectral data obtained, showing the predominance of the thione form in these solvents, a DFT theoretical study on a similar thioamide N-heterocyclic ligand has been recently carried out [19]. The latter confirms the stability of the thione tautomeric form compared to the thiol one, in both gaseous phase and aqueous medium. In order to confirm the dominance of the thione tautomeric form of the ligand in the solid state, a careful examination of the most important bands has been made [20], υ(O–H) 3496 cm^{-1}, υ(C=O)

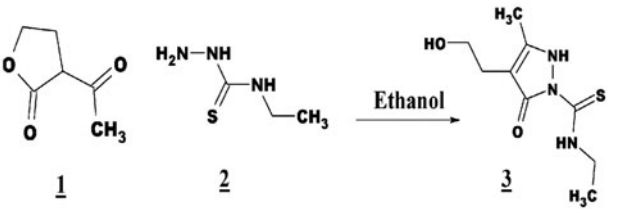

Scheme 1. Synthesis of the ligand H2L.

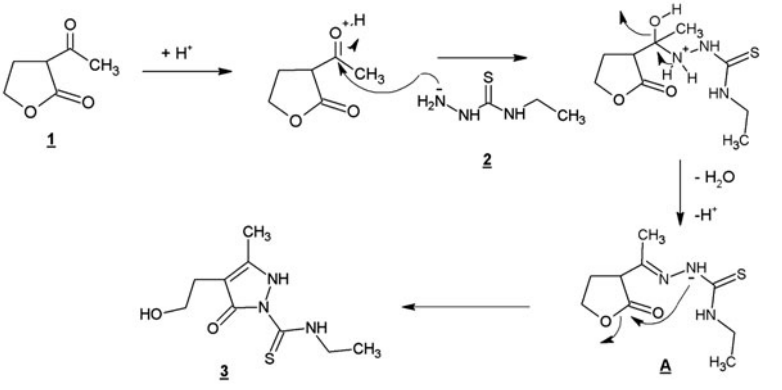

Scheme 2. Mechanism of the synthesis.

1639 cm^{-1}, υ(C=C) 1548 cm^{-1}, υ(C–O) 1049 cm^{-1}, and υ(C=S) 789 cm^{-1}. The band corresponding to υ(S–H) at 2380–2400 cm^{-1} is absent from the IR spectrum of the ligand which indicates that the thione form is dominant in the solid state.

2.2.2. Synthesis of Cu(II) and Ni(II) complexes. An ethanolic solution containing 0.25 mmol (0.043 g) of $CuCl_2{\cdot}2H_2O$ was mixed with another one containing 0.5 mmol (0.115 g) of **3** also dissolved in ethanol. The mixture which turned immediately deep brown was stirred and refluxed for 3 h. The resulting solid was recrystallized with ethanol and deep brown crystals suitable for single-crystal X-ray study have been obtained. Yield: 80%. The Ni(II) complex was prepared by a similar procedure to that of the Cu(II) complex using $NiCl_2{\cdot}6H_2O$ salt (0.059 g). After slow evaporation of the solvent, the solid was washed with ethanol and green crystals also suitable for single-crystal X-ray study were obtained. Yield: 50%.

2.3. *Potentiometric study*

2.3.1. pH-metric titration procedure. The pH-metric readings were measured to 0.01 unit with a Schott Titroline Easy Model, standardized before titrations with buffer solutions produced by Fluka. All the solutions were introduced into a thermostated double-walled electrochemical cell that maintains a constant temperature (25 ± 0.1 °C). The titrations were conducted under nitrogen in order to avoid interference with CO_2 or O_2 gasses.

The following solutions were prepared in (90 : 10 v/v) water/ethanol and 0.2 M ionic strength (NaCl) and titrated against carbonate free NaOH 0.1 M as follows: (i) the solvent is 20 mL of NaCl (0.5 M) with 5 mL of absolute ethanol and completed to 50 mL in a volumetric flask with distilled water, (ii) ligand solution is 20 mL of NaCl (0.5 M) with 5 mL of the ligand (5×10^{-3} M) and 5 mL of HCl (0.1 M) completed to 50 mL, and (iii) metal–ligand solution is 20 mL of NaCl (0.5 M) with 5 mL of the ligand (5×10^{-3} M), 5 mL of Cu^{2+} or Ni^{2+} solutions (2.5×10^{-3} M) and 5 mL of HCl (0.1 M) completed to 50 mL with distilled water.

2.3.2. Method for computing the constants. The potentiometric measurements are exploitable by Sirko program [21], which first calculates from the titration of the mixture (90 : 10 v/v) water/ethanol at 0.2 M ionic strength the correction factor in the pH-reading. As the conventional pH range is based on the dissociation behavior of water, the composition of a new mixture may have a relevant ion product and not water's. The pH-meter readings pH* in the mixture used in this work differs by 0.02 from the corrected reading in aqueous medium [22].

$$\mathrm{pH}^* = \mathrm{pH} - \delta$$

Consequently, the presence of 10% ethanol has a minor influence on the dissociation and stability constants. The dissociation constants of the ligand are then calculated and used with the potentiometric data of the two complexes in order to have their stability constants and the species distribution curves.

2.4. *X-ray crystallography*

Crystallographic studies of the Cu(II) and Ni(II) complexes (**A** and **B**, respectively) were performed at 170 K using an Oxford Diffraction Xcalibur 2-CCD diffractometer fitted with graphite monochromated Mo$K\alpha$ radiation ($\lambda = 0.71073$ Å).

Small crystals, $0.18 \times 0.09 \times 0.08$ mm^3 for **A** and $0.12 \times 0.07 \times 0.06$ mm^3 for **B**, were used to collect data. The full sphere data collections were performed using 0.75° ω-scans with an exposure time of 25 s for **A**, 1.0° ω-scans with an exposure time of 60 s per frame for **B**. Data collection and data reduction were done with the CRYSALIS-CCD and CRYSALIS-RED programs on the full set of data [23]. For both complexes, the crystal structures were solved by direct methods and successive Fourier difference syntheses using the Sir92 program [24] and refined on F^2 by weighted anisotropic full-matrix least-square methods using SHELXL97 [25]. Both programs were used within the WINGX package [26]. All nonhydrogen atoms were refined anisotropically. Except hydrogens attached to N3, O1, and O2 (H3, H1, and H2, respectively) which were located by difference Fourier map, all other hydrogens were calculated and included as isotropic fixed contributors to F_c. All other calculations were performed with standard procedures (WINGX) [26].

2.5. *Electrochemistry*

Cyclic voltammetry experiments were conducted at room temperature with analyte concentrations of 1 mM in DMSO using 0.1 M tetrabutylammonium hexafluorophosphate (Aldrich) as the supporting electrolyte. All solutions were purged at least 15 min with N_2.

The three-electrode system consisted of a glassy carbon-working electrode, platinum auxiliary, and Pt reference electrodes. The ferrocenium/ferrocene couple, which was added at the end of each experiment, was used to monitor the reference electrode and was observed at 0.48 V with $\Delta E_p = 0.140$ V under these conditions. All potentials are given against ferrocene. In order to understand the redox chemistry of H_2L, and its corresponding complexes, cyclic voltammetric studies have been conducted from +3.0 to −3.0 V.

2.6. *DNA-binding experiments*

2.6.1. UV–vis experiments. Transition metal complexes can bind to DNA via both covalent and/or noncovalent interactions. In the case of covalent interaction, the labile ligand of the complex can be replaced by a nitrogen base of DNA such as guanine N7.

The noncovalent interactions include intercalative, electrostatic, and groove (surface) binding of metal complexes outside of the DNA helix [27]. The changes observed in the UV spectrum upon titration may give evidence of the existing interaction mode. Since hypochromism due to $\pi \rightarrow \pi$ stacking interactions may appear in the case of the intercalative binding mode, and a red shift (bathochromism) may be observed when the DNA duplex is stabilized [28].

The UV spectrum of each complex has been recorded in buffer (15 mM of trisodium citrate and 150 mM of NaCl at pH 7.2) in the presence of 1% DMSO. UV titrations have been conducted for a constant concentration of each complex (20 μM) in the presence of increasing amounts of DNA in buffer (concentrations varying from 2 to 30 μM). Measurements have been conducted after addition of equal amounts of FS-DNA in both the sample solution and the reference one in order to avoid the absorbance of FS-DNA itself.

2.6.2. Cyclic voltammetry experiments. The interaction of DNA with the complexes by cyclic voltammetry was conducted in the same conditions of degasification and room temperature using the buffer solution (15 mM of trisodium citrate and 150 mM of NaCl) as solvent with the supporting electrolyte. The saturated Ag/AgCl/KCl was used as the reference electrode and 10^{-3} analyte solutions were prepared in the mixture (buffer/DMSO) (90%/10%); 10% of DMSO was necessary to solubilize **A** and **B**.

2.7. *Physical measurements*

^{1}H NMR and ^{13}C NMR spectra were recorded on a 300 MHz and 75 MHz spectrometer. Chemical shifts are quoted in parts per million (ppm) referenced to tetramethylsilane. Mass spectra were recorded with a Varian MAT 311 instrument by the Center Régional de Mesures Physiques de l'Ouest, Rennes. IR spectra were recorded on a Perkin Elmer Spectrum One FTIR spectrophotometer with KBr disks from 4000 to 400 cm^{-1}. Electronic spectra were recorded in ethanol or DMSO on a Jasco V530 UV-Visible (200–1100 nm) spectrophotometer using quartz cells. Magnetic susceptibility measurements were carried out with applied magnetic field of 0.1 T on polycrystalline samples of **A** and **B** with a Quantum Design MPMS-XL-5 SQUID magnetometer.

X-band EPR measurements were carried out on a Bruker ELEXSYS 500 spectrometer with a maximum available microwave power of 200 mW and equipped with a super-high-Q resonator ER-4123-SHQ and standard Oxford Instruments low temperature devices.

For Q-band studies, EPR spectra were recorded on a Bruker EMX system equipped with an ER-510-QT resonator. The magnetic field was calibrated by an NMR probe and the frequency inside the cavity was determined with a Hewlett-Packard 5352B microwave frequency counter. Computer simulation: WINEPR-Simfonia, version 1.5, Bruker Analytische Messtechnik GmbH). Experiments of cyclic voltammetry were conducted using a potentiostat/galvanostat Autolab PGSTAT302 Metrohm.

3. Results and discussion

3.1. *Potentiometric study*

The values of the overall dissociation constants of the ligand, $-\log \beta_q$ according to the following equilibrium, are listed in table 1 with the calculated stepwise dissociation constants p*K*i.

$$\left[H_qL\right]^{q-2} \rightleftharpoons q\ H^+ + \ L^{2-}$$

The stability constants of Cu(II) and Ni(II) complexes at 298 K and 0.2 M ionic strength are summarized in table 2. Ligand and metal species distribution curves are given in figures 1–3.

The ligand exhibits four deprotonations associated with the three amino moieties and the alcohol. The first and second dissociation constants, $pK_1 = 2.44$ and $pK_2 = 2.48$, can be respectively attributed to deprotonation of the heterocyclic nitrogen involved in the thioamide group (N1) and to the aliphatic nitrogen also involved in the thioamide moiety (N3). These amino groups have been previously protonated by hydrochloric acid.

$$H_4L^{2+} \rightleftharpoons H^+ + H_3L^+$$

$$H_3L^+ \rightleftharpoons H^+ + \ H_2L$$

Table 1. Dissociation constants of the ligand in (90 : 10 v/v) H_2O/EtOH at 298 K and 0.2 M ionic strength.

H_2L	$-\log \beta_1 = 2.48$	$pK_1 = 2.48$
	$-\log \beta_2 = 4.92$	$pK_2 = 2.44$
	$-\log \beta_3 = 11.57$	$pK_3 = 6.65$
	$-\log \beta_4 = 21.48$	$pK_4 = 9.90$

Table 2. Stability constants of Cu(II) and Ni(II) complexes in (90 : 10 v/v) H_2O/EtOH at 298 K and 0.2 M ionic strength.

Complexes	$\log \beta_i$	$\log K_i$
$[Cu(HL)]^+$	22.45 ± 0.01	22.45
$[Cu(HL)_2]$	33.36 ± 0.02	11.90
$[Ni(HL)]^+$	13.67 ± 0.07	13.67
$[Ni(HL)_2]$	22.79 ± 0.10	09.12

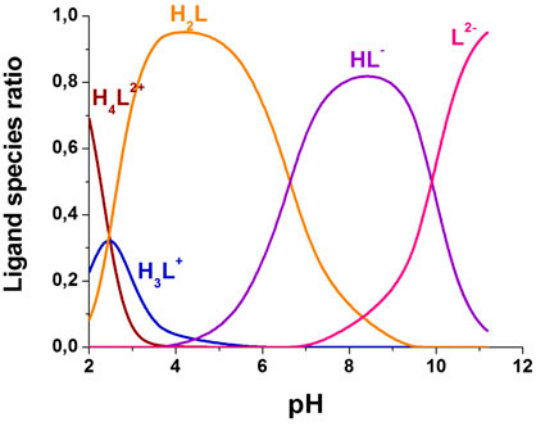

Figure 1. Distribution curve of ligand's species.

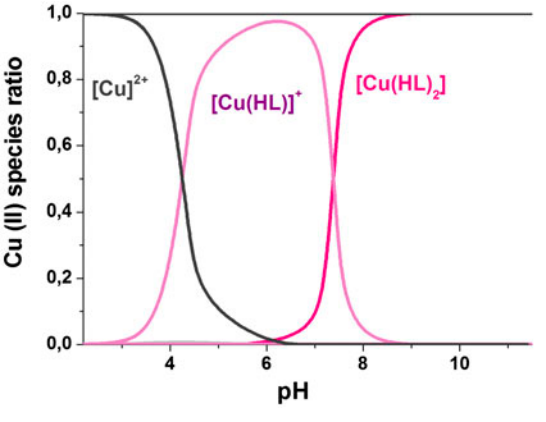

Figure 2. Distribution curve of Cu(II) species.

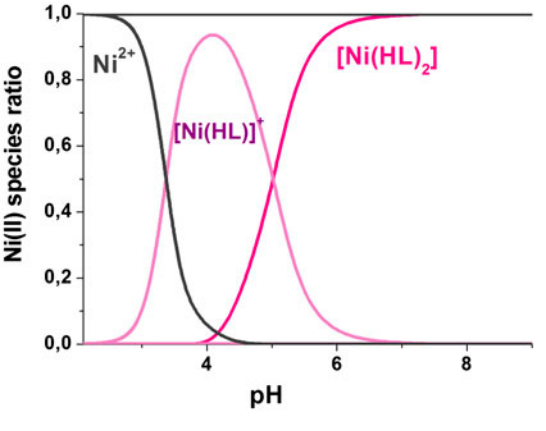

Figure 3. Distribution curve of Ni(II) species.

The third deprotonation constant, $pK_3 = 6.65$, is attributed to the dissociation of the nitrogen (N2) bound to the metal in the complex. The last one, $pK_4 = 9.90$, corresponds to the deprotonation of the alcohol group.

$$H_2L \rightleftharpoons H^+ + HL^-$$

$$HL^- \rightleftharpoons H^+ + L^{2-}$$

These results are in agreement with the ones given for parent molecules in similar experimental conditions [19].

From the data depicted in table 2, both copper(II) and nickel(II) complexes show high stability constants, revealing the ligand ability to complex. These stable species are the synthetized ones in the solid state. As expected, log K_1 of $[Cu(HL)_2]$ is higher than log K_1 of $[Ni(HL)_2]$, which is in accord with the Irving–Williams series.

3.2. *Crystal structures*

Crystallographic analysis of $[M(HL)_2(H_2O)]\cdot 2H_2O$ (M(II) = Cu (**A**) and Ni (**B**)) reveals that the compounds are isostructural and crystallize in the centrosymmetric monoclinic *C2/c* space group. Crystallographic data and selected bond lengths and angles are listed in tables 3 and 4, respectively. The asymmetric unit contains a metal ion and a coordinated water,

Table 3. Crystal data and structural refinement parameters for **A** and **B**.

	A	**B**
Empirical formula[a]	$C_{18}H_{34}CuN_6O_7S_2$	$C_{18}H_{34}N_6NiO_7S_2$
Molecular weight	574.17	569.34
Space group	*C2/c*	*C2/c*
a (Å)	16.2871(5)	16.4180(6)
b (Å)	16.6739(7)	16.7700(5)
c (Å)	10.4510(4)	10.4530(4)
β (°)	116.869(7)	117.754(5)
V (Å^3)	2531.77(16)	2546.92(15)
Z[a]	4	4
ρ_{calcd} (g cm^{-3})	1.506	1.485
μ (cm^{-1})	10.77	9.75
F (0 0 0)	1204	1200
Crystal size (mm)	0.18 × 0.09 × 0.08	0.12 × 0.07 × 0.06
Reflections measured	8789	10,139
2θ range (°)	6.56–54.00	6.56–54.00
Reflections unique/R_{int}	2756/0.0349	2775/0.0346
Reflections with $I > 2\sigma(I)$	2349	2199
N_v	164	164
R_1[b]/wR_2[c]	0.0360/0.1034	0.0358/0.1000
GooF[d]	1.055	1.010
$\Delta\rho_{max,\ min}$ (e Å^{-3})	+0.808/−0.379	+0.572/−0.396

[a]The asymmetric unit contains 0.5 of the chemical formula.
[b]$R_1 = \sum |F_o - F_c| / F_o$.
[c]$wR_2 = \left\{ \sum \left[w(F_o^2 - F_c^2)^2 \right] / \sum \left[w(F_o^2)^2 \right] \right\}^{\frac{1}{2}}$.
[d]$\text{GooF} = \left\{ \sum \left[w(F_o^2 - F_c^2)^2 \right] / (N_{obs} - N_{var}) \right\}^{\frac{1}{2}}$.

Table 4. Selected bond lengths (Å) and angles (°) in **A** and **B**.

	A (M = Cu^{II})	**B** (M = Ni^{II})
M–N2	1.9481(18)	2.0120(17)
M–O2	2.123(3)	2.020(3)
M–S1	2.3729(6)	2.3457(6)
N3–C7	1.316(3)	1.314(3)
N1–C7	1.375(3)	1.378(3)
N1–N2	1.389(2)	1.386(2)
N1–C1	1.414(3)	1.414(3)
N2–C3	1.333(3)	1.332(3)
S1–C7	1.694(2)	1.699(2)
C2–C1	1.395(3)	1.391(3)
$N2^{(i)}$–M–N2	179.05(10)	176.92(10)
N2–M–O2	90.47(5)	91.54(5)
$N2^{(i)}$–M–S1	95.47(6)	94.75(5)
N2–M–S1	84.09(6)	83.59(5)
O2–M–S1	117.655(17)	122.547(18)
S1–M–$S1^{(i)}$	124.69(3)	114.91(4)

Note: Codes of equivalent position (i): -*x*+1, *y*, -*z*+1/2.

both located on the special position (1/2 y 1/4), a HL^- chelating ligand and two uncoordinated water molecules, located on general positions (figures 4 and 5), giving the formula $[M(HL)_2(H_2O)]\cdot 2H_2O$ (M = Cu^{II} (**A**) and Ni^{II} (**B**)).

Careful examination of the crystallographic data of the anionic ligand reveals that central fragment (O4C1C2C3N2N1C7S1N3) in both complexes is nearly planar with a maximum deviation of 0.005 Å in **A** and 0.022 Å in **B**. This planar geometry can be explained by electronic delocalization between all atoms of this central unit as clearly shown in scheme 3.

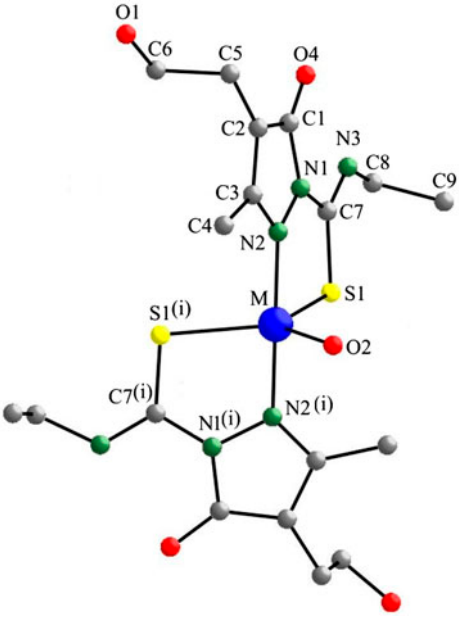

Figure 4. Molecular structure of the discrete complexes of **A** and **B** showing the asymmetric unit, the atom labeling scheme and the coordination environment of the metal ion. Codes of equivalent position: (i) $-x + 1, y, -z + 1/2$.

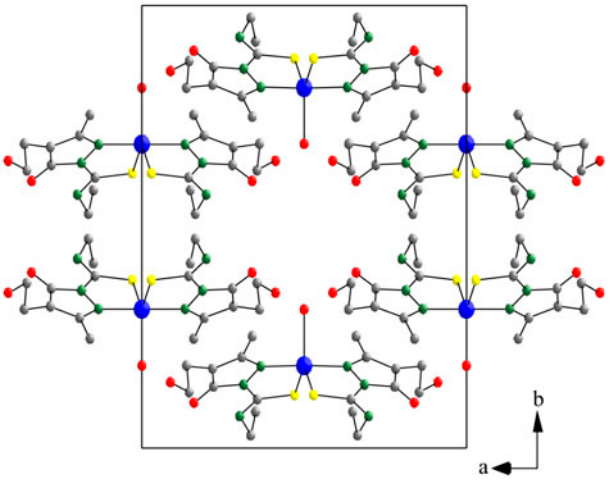

Figure 5. Projection view of the overall structure of **A** and **B** along the [0 0 1] direction.

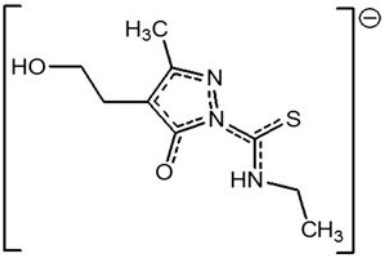

Scheme 3. Electronic delocalization in the anionic $[HL]^-$ ligand.

The three carbons C1, C2 and C3 and N1 and N3 (figure 4) have sp^2 hybridization, as indicated by the sum of the three angles around them (359.7–360.0° for **A** and **B**).

Additional proof of the electron delocalization over the central fragment comes from the C–C, C–N, N–N, C–O and C–S bond distances (table 4), which are longer than a normal double bond but much shorter than single bonds, suggesting that the nine bond lengths of this central fragment present partial double character.

For each compound, the metal ion has a $[M(SN)_2O]$ environment arising from two nitrogens and two sulfurs (N2, $N2^{(i)}$, S1 and $S1^{(i)}$) of two equivalent chelating HL^- anionic ligands, and from one water (O2). As clearly depicted in figure 4, both metal ions are located in almost perfect trigonal bipyramidal geometries as indicated by the high value of the trigonality index, τ [29], of 0.906 for both metal ions [$\tau = (\beta - \alpha)/60$, where α and β (in °) are the two greatest basal plane angles when the polyhedron is viewed as a square pyramid; for a perfectly square-pyramidal geometry, τ is equal to zero and becomes unity for a perfectly trigonal bipyramid geometry]. In the trigonal bipyramids, the equatorial plane involves S and $S^{(i)}$ arising from the two equivalent HL^- chelating ligands and the coordinated water (O2). The two apical positions are occupied by nitrogens from the two chelating ligands (N2 and $N2^{(i)}$). Although the trigonal bipyramidal structure is relatively

unusual for Ni(II), it has been reported for similar ligands, such as some tridentate thiosemicarbazides, that are known to coordinate generally via N_2,S donor sets [30]. The trigonal bipyramidal structure has also been reported for Cu(II) in the case of parent molecules such as thioamidopyridine derivatives with a similar S,N-chelation [31]. As expected (table 4), Cu–O2 and Cu–S1 bonds are longer than Ni–O2 and Ni–S1, as a result of Jahn–Teller effect on the Cu(II) complex.

Relatively little attention has been paid to Jahn–Teller effect in copper(II) compounds having stereochemistries other than cubic ones despite the fact that it can play a fundamental role in the crystal structure and the spectroscopic behavior of five-coordinate cupric compounds [32].

3.3. *IR spectral study*

A careful examination of IR spectra of Cu(II) and Ni(II) complexes, and a comparison with the ligand, shows that the band corresponding to C=S stretch is affected by complexation and shifts to lower frequencies by 15 cm^{-1} in both complexes. A broad band at 3200–3400 cm^{-1} due to coordinated water, and Cu–O and Ni–O vibrations, appear at 457 and 407 cm^{-1}, respectively. The IR spectra show new bands at 462 and 472 cm^{-1} that can be assigned to υ(Cu–N) and υ(Ni–N).

3.4. *Electronic spectral study and magnetic moments*

The electronic spectral features of the ligand and its complexes in absolute ethanol and their magnetic moments are summarized in table 5. The electronic spectrum of the ligand shows a shoulder at 300 nm and two bands at 277 nm and 239 nm; all correspond to $\pi \rightarrow \pi^*$ transitions.

The magnetic moment of $[Cu(HL)_2H_2O]$ at 300 K is 1.79 B.M., which is in the range of the expected value for spin only moment for one unpaired electron. The electronic spectrum of $[Cu(HL)_2H_2O]$ exhibits a band at 734 nm and a shoulder at 500 nm, arising from d–d transitions. The first band is assignable to $^2A_1' \rightarrow {}^2E'$ transition and the second one to $^2A_1' \rightarrow {}^2E''$ transition [33] (figure 6), arising from the d^9 configuration of Cu(II) in a trigonal bipyramidal crystal field (D_{3h}). The spectrum of the green $[Ni(HL)_2H_2O]$ exhibits four bands and a shoulder: a first band at $\lambda > 1100$ nm (upper limit of the wavelength range of the spectrophotometer), three other bands at 669, 399, and 389 nm, and the shoulder at 385 nm, all arising from d–d transitions.

Table 5. Magnetic moments at 300 K and electronic spectra of the ligand, Cu(II) and Ni(II) complexes.

	λ (nm)	υ (cm^{-1})	ε (l cm^{-1} mol^{-1})	Assignment	μ_{eff} (B.M.)
H_2L	300	33,333	33,333	$\pi \rightarrow \pi^*$	–
	277	36,101	36,223	$\pi \rightarrow \pi^*$	
	239	41,841	41,847	$\pi \rightarrow \pi^*$	
$[Cu(HL)_2(H_2O)]\cdot 2H_2O$	734	13,624	490	$^2A_1' \rightarrow {}^2E'$	1.79
	500	20,000	606	$^2A_1' \rightarrow {}^2E''$	
$[Ni(HL)_2(H_2O)]\cdot 2H_2O$	>1100	<9000	~25	$^3E' \rightarrow {}^3E''$	4.19
	669	14,948	59	$^3E' \rightarrow {}^3A_2'$	
	399	25,063	178	$^3E' \rightarrow {}^3A_1'' + {}^3A_2''$	
	389	25,707	365	$^3E' \rightarrow {}^3E''$	
	385	25,974	1099	$^3E' \rightarrow {}^3A_2'$	

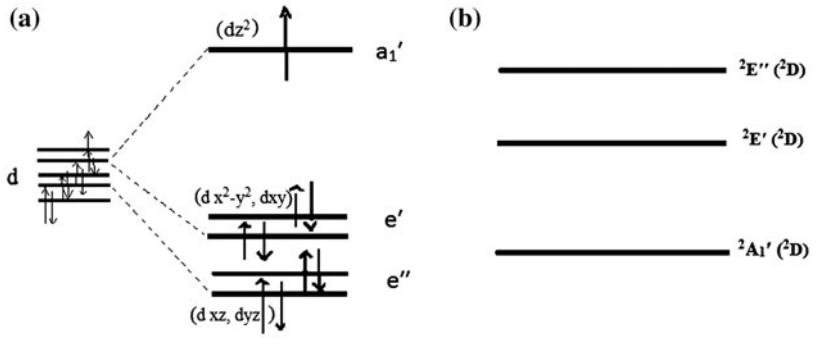

Figure 6. Electronic structure of Cu(II) in a trigonal bipyramidal crystal field (D_{3h}) (**a**) fundamental electronic configuration and (**b**) energy levels.

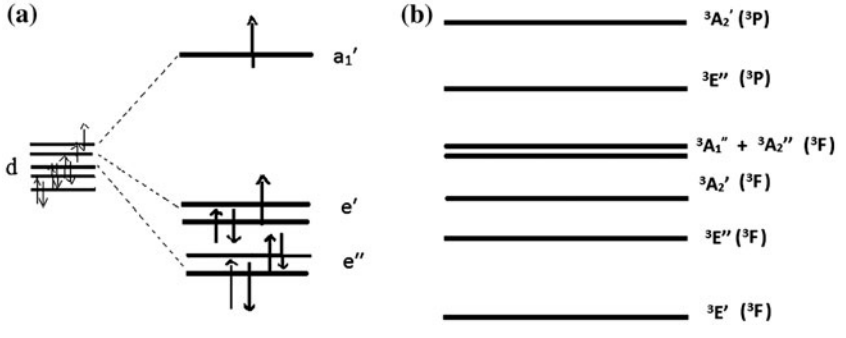

Figure 7. Electronic structure of Ni(II) in a trigonal bipyramidal crystal field (D_{3h}) (**a**) fundamental high spin configuration and (**b**) energy levels.

In a trigonal bipyramidal crystal field symmetry, five spin-allowed transitions are expected for high spin Ni(II) and only two for a low spin [33, 34]. The electronic spectrum of Ni(II) complex indicates that the electronic fundamental configuration is the high spin one (figure 7), which is in agreement with the magnetic moment of 4.19 M.B. (table 5). This value is expected for a double degenerate electronic ground level E', for which a strong contribution of the orbital moment occurs [35].

3.5. *EPR measurements*

X and Q band EPR measurements were carried out on powdered samples at several temperatures from 5 to 300 K. The X-band EPR spectra exhibit near axial symmetries for the g tensor in the $DM_s = \pm 1$ region, but an appreciable extent of rhombicity can be detected operating at the Q–band (figure 8). The spin Hamiltonian parameters were estimated by the comparison of the experimental spectra with those obtained by a computer simulation program working at the second order of perturbation theory. The parameters were then optimized by trial and error and the best-fit result is represented as the dashed line in figure 8.

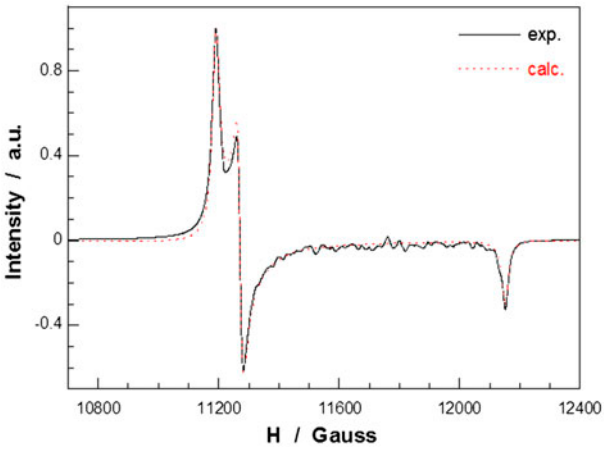

Figure 8. Room temperature Q-band EPR spectrum of **A**. Dashed line is the best fit; see text for the fitting parameters.

The calculated g values are $g_1 = 2.006$, $g_2 = 2.163$, and $g_3 = 2.178$ that could be described as "inverse or reversed" axial g values ($g_\perp > g_\| > 2.0023$) according to the Hathaway and Billing classification [36]. This sequence of values can indicate that the unpaired electron is located in the d_{z2} orbital, in agreement with the geometry near trigonal bipyramidal of the CuN_2S_2O chromophore at room temperature (Addison parameter $t = 0.92$), and with the electronic structure proposed in figure 6. However, this result must be cautiously evaluated. Electron pair repulsion calculations for five-coordinate Cu(II) complexes show that the energetically most favorable coordination geometry is an elongated trigonal bipyramid with a mainly d_{z2} ground state [37]. However, the majority of the studied "CuL_5" complexes exhibit the "usual" g value sequence ($g_\| > g_\perp > 2.0023$) and present geometries near to elongated square pyramids due to steric effects and vibronic couplings [38]. Moreover, many "reversed" EPR spectra correspond to d_{x2-y2} ground states that are masked by exchange effects or dynamic average over differently oriented elongated square pyramids [39, 40]. Therefore, correlation with other physical techniques and/or variable temperature EPR experiments is usually needed to unambiguously determine the ground state of the complexes.

Molecular g values directly reflect the ground state wave function of an unpaired electron. In particular, for a five-coordinate Cu^{2+} polyhedron:

$$g_z = g_0 + \frac{8c^2}{1+c^2}\,u_z$$

$$g_y = g_0 + \frac{2c^2}{1+c^2}\left(1 \mp \frac{\sqrt{3}}{c}\right)^2 u_y$$

$$g_x = g_0 + \frac{2c^2}{1+c^2}\left(1 \pm \frac{\sqrt{3}}{c}\right)^2 u_x$$

The orbital contributions u_i are defined as follows:

$$u_{\mathrm{i}} = \frac{k_{\mathrm{i}}^2 \lambda_0}{\Delta E_{\mathrm{i}}} \quad (i = z, y, x)$$

where λ_0 is the spin–orbit coupling constant for a free Cu^{2+} (equal to $-830\ \mathrm{cm}^{-1}$), k_{i} is the spin–orbit reduction parameter (covalency factor) and ΔE_{i} energy refers to the d–d transitions. As the mixing coefficient c becomes null in a perfect trigonal bipyramid:

$$g_{\mathrm{z}} = g_{||} = g_0$$

$$g_{\mathrm{x}} = g_{\mathrm{y}} \equiv g_{\perp} = g_0 - \frac{6k_{\perp}^2 \lambda_0}{\Delta E(^2A_1' \rightarrow {}^2E')}$$

Using the experimental g values and the energy splitting ΔE determined from the electronic spectra, a covalency factor of $k_{\perp} = 0.82$ is obtained, which is reasonable for a complex where the coordination sphere contains S, O, and N donors.

If the molecular motions are not restricted to one of the minima of the ground-state potential energy, which may occur near room temperature, the g values can be also related to the orbital contributions but with different equations to those used above. In the particular case of a dynamic delocalization of the electron over the xy-plane, motional narrowing in the EPR spectra also induces a "reversed" signal but with the following g values:

$$g_{||}^{\mathrm{dyn}} = g_0 + 2u\perp$$

$$g_{\perp}^{\mathrm{dyn}} = g_0 + 4u_{||} + 2u\perp$$

However, for realistic k and ΔE values, the lowest g value always exceeds 2.04, significantly larger than the experimentally observed 2.006. Moreover, the EPR spectrum remains practically unchanged over the studied temperatures, hence any dynamic Jahn–Teller effect can be ruled out. Furthermore, while no splitting due to copper nuclear spins is observed, the three peaks corresponding to the main components of the g tensor are clearly resolved with surprisingly small line-widths, approximately 15 Gauss (full width at half-height in the derivative spectra). The absence of hyperfine lines in such a system, together with the Lorentzian form of the lines, implies that magnetic exchange is present in this compound, in spite of the large distances between copper ions and the absence of a covalent skeleton connecting them. Taking into account that the observed g values are in agreement with the coordination sphere of the Cu^{2+} ions and the d_{z2} ground-state wave function, only interactions between magnetically equivalent molecules are operative. Consequently, some narrowing of the linewidth and the collapse of the hyperfine structure are observed, but the molecular g values remain unaffected. The magnetic effective moment that can be deduced from the determined g values (1.83 B.M.) compares rather well with that experimentally obtained from magnetic measurements (1.79 B.M.).

Considering the structural features of the compound, the collapse of all the EPR individual resonances must involve magnetic interactions propagated via H bonds among ordered chromophores with the same orientation. This "ferrodistortive" order, together with the rigid ligand effect, must be responsible for stabilizing the compressed trigonal bypyramid geometry in this compound instead of the usually more stable elongated square

pyramidal. It appears that, although weak, the magnetic interactions are strong enough to determine the molecular structure of the compound and therefore its electronic properties.

3.6. *Electrochemistry*

Cyclic voltammograms of **A** and **B** are reported in figures 9 and 10. A rigorous examination of the ligand's voltammogram reveals two irreversible oxidation processes occurring at 0.50 and 0.80 V. This suggests formation of stable oxidized species. The voltammogram also exhibits a broad cathodic peak at −2.70 V assignable to reduction of an unsaturated group of the ligand.

The cyclic voltammogram of **A** reveals one more irreversible oxidation peak at −0.20 V that can be assigned to the oxidation of Cu(II) to Cu(III). A cathodic peak also appears at −1.60 V, which is believed to be the reduction of Cu(II) to Cu(I) [41]. The broad cathodic peak of the ligand is affected by complexation and shifted to more positive potentials; this suggests that the reduction is more easily accomplished in the complex than in the free ligand.

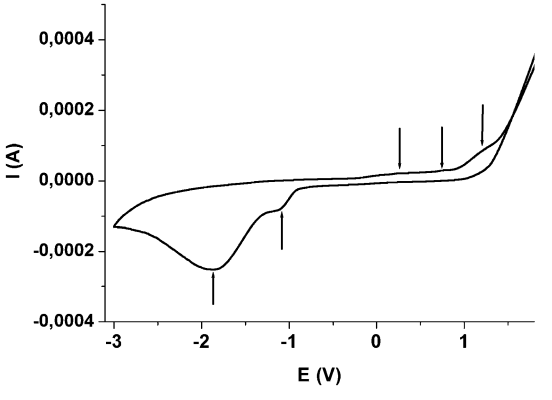

Figure 9. Cyclic voltammogram of $[Cu(HL)_2(H_2O)]$ 10^{-3} M in DMSO (200 mV s^{-1} scan rate). The arrows show the peak positions.

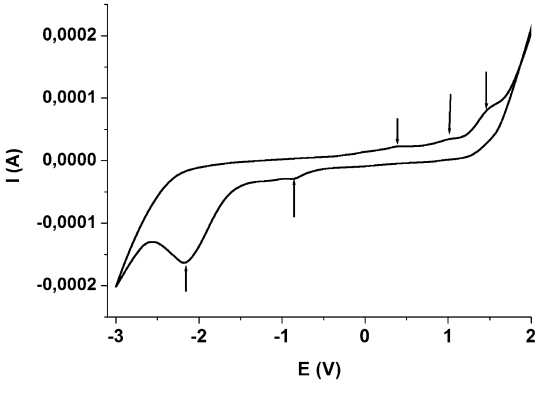

Figure 10. Cyclic voltammogram of $[Ni(HL)_2(H_2O)]$ 10^{-3} M in DMSO (200 mV s^{-1} scan rate). The arrows show the peak positions.

The voltammogram of **B** also exhibits an irreversible anodic process at around −0.1 V, which is assigned to the oxidation of Ni(II) to Ni(III). A cathodic peak that appears at −1.3 V is believed to be the reduction of Ni(II) to Ni(I) [42]. The irreversibility of all these processes is indicated by the high values of the peak-to-peak separation.

3.7. *Interaction with FS-DNA*

3.7.1. FS-DNA binding studied by UV experiments. UV spectra of **A** and **B** have been recorded in the absence and presence of increasing amounts of DNA. Figure 11 shows the changes upon titration. Any interaction between each complex and DNA could perturb the intraligand bands during these titrations [28].

The intense band λ_{max} that appears at 249 nm in **A** and 246 nm in **B** ($\pi \rightarrow \pi^*$ intraligand transitions) have been chosen to monitor the changes upon titration. Cu(II) and Ni(II) complexes exhibited the same changes. Addition of increasing amounts of DNA resulted in a clear reduction of absorbence, a hypochromism without any shift in the maximum absorbance wavelength.

Normally, a compound bound to DNA through intercalation results in hypochromism with or without a blue/red shift [43]. Certain aromatic planar chemicals bind to DNA by intercalation. In this process, the compound inserts between two stacked base pairs of DNA and positions itself within the center of the DNA double helix. The intercalated molecule is stabilized by hydrophobic stacking interactions with adjacent base pairs [44]. The magnitude of the binding strength of the complexes with FS-DNA can be evaluated by the value of the binding constant K_b. The latter is calculated by the Wolfe–Shimer equation [45]:

$$[\mathrm{DNA}]/(\varepsilon_a - \varepsilon_f) = [\mathrm{DNA}]/(\varepsilon_b - \varepsilon_f) + 1/\mathrm{K_b}(\varepsilon_b - \varepsilon_f)$$

with ε_a being the apparent absorption coefficient corresponding to A_{obs}/[compound], ε_f the absorption coefficient of the free compound, and ε_b the absorption coefficient of the compound when fully bound to DNA. K_b is obtained by the ratio of slope to Y intercept in plots of [DNA]/(ε_a–ε_f) *versus* [DNA] (figure 11). The K_b values of **A** and **B** are $0.7 \times 10^4\ M^{-1}$ and $1.65 \times 10^4\ M^{-1}$, respectively. [Ni(HL)$_2$(H$_2$O)] exhibits a constant twice larger than [Cu(HL)$_2$(H$_2$O)], indicating better binding with DNA.

Many copper(II) complexes have been reported with moderate to good binding affinity with DNA [46–48]. Different interaction modes are reported, groove binding [49, 50] and intercalation the most observed [46, 47]. Many parameters are to be considered in the strength of the binding in the case of the intercalation. Among the most important ones is the planarity of the ligands.

Many previous studies on complexes containing large delocalizations, or aromatic rings as in the present work (see scheme 3), show that larger is the planarity of the ligands, better is the binding affinity [47–51]. However, this cannot be a rule, as some highly aromatic planar ligands show moderate binding strength [52].

A comparison between the binding constant of **B** with some previously reported Ni(II) complexes with a comparable $N_2S_2O_2$ coordination environment shows that **B** exhibits a smaller binding constant, mainly because of larger planarity exhibited by ligands in the reported complexes, and in some cases, because of the presence of a withdrawing element on the ligand which is believed to enhance the binding affinity [53].

However, the binding constants of **A** and **B** are comparable to similar complexes of N-donor and N,S-donor ligands [53, 54], and are within the range 103–104 M^{-1}, which

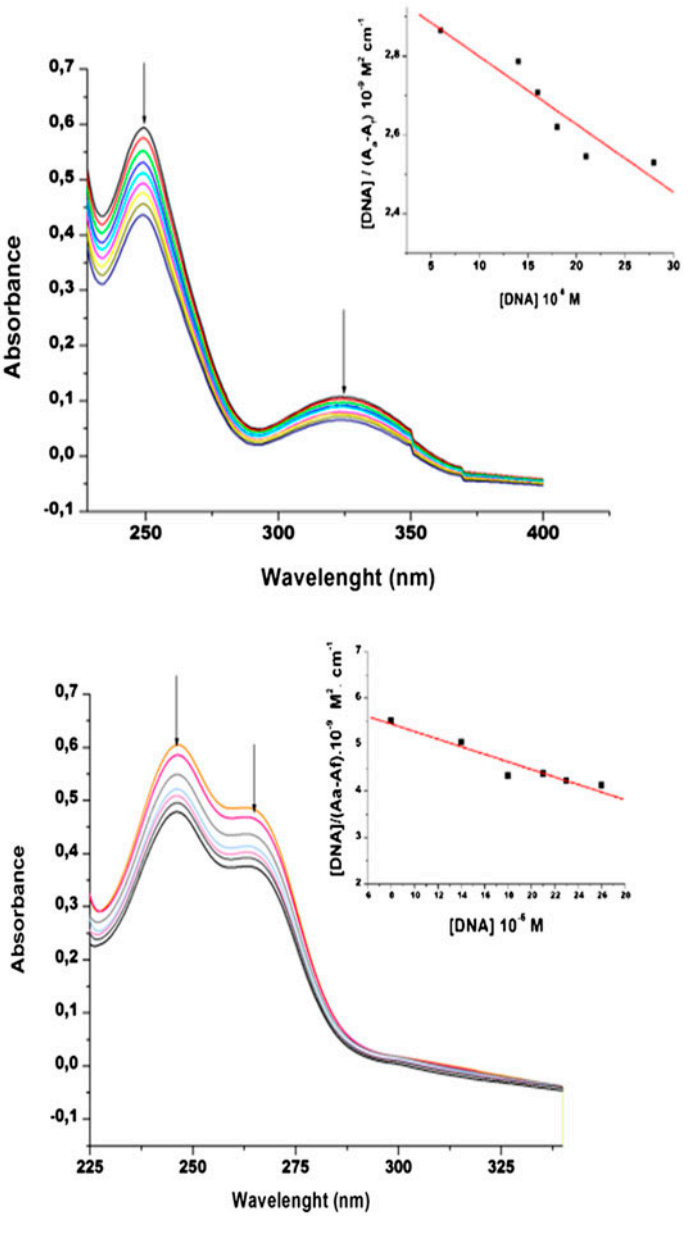

Figure 11. UV spectra of 20 μM in buffer (containing 1% DMSO) of $[Cu(HL)_2H_2O]$ and $[Ni(HL)_2H_2O]$, respectively, in the absence and presence of increasing amounts of DNA. In plot: $[DNA]/(\varepsilon_a - \varepsilon_f)$ *vs*. [DNA].

makes them moderate intercalators, smaller than the conjugated classical intercalator Ethidium Bromide (K_b = 1.23 (±0.07) × 10^5 M^{-1}) [55].

3.7.2. FS-DNA binding studied by cyclic voltammetry. The electrochemical investigations of metal–DNA interactions provide a useful supplement to spectroscopic methods and

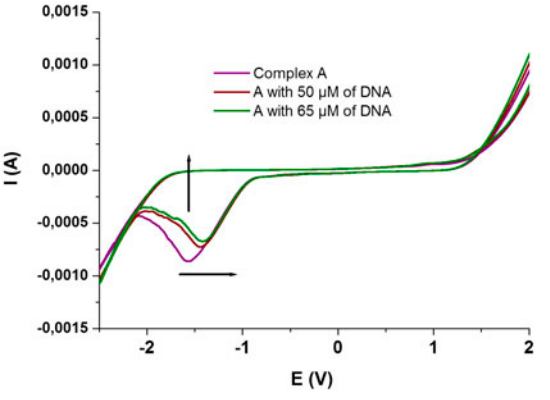

Figure 12. Cyclic voltammogram of **A** 10^{-3} M in (90%/10%) buffer/DMSO in the absence and presence of increasing amounts of DNA (scan rate = 200 mV s^{-1}). Arrows show the changes upon titration.

yield information about the interaction mode. The cyclic voltammogram of **A** upon addition of FS-DNA, chosen to show the changes, is given in figure 12.

A careful examination of the voltammograms in the buffer solution (15 mM of trisodium citrate and 150 mM of NaCl) shows the same redox processes as previously reported from the electrochemical study in DMSO, although one can notice decrease in intensity of some peaks.

No additional redox peaks appear upon addition of FS-DNA, but all the peaks are affected and shift toward more positive values of potentials as depicted in figure 12. (The broad cathodic peak is chosen to monitor the changes for clarity). Both cyclic voltammograms of **A** and **B** show a decrease in the current intensities, explained by an equilibrium mixture at the surface of the electrode of the free, and the DNA-bound complex [56].

In general, the electrochemical potential of a small molecule will shift positively when it intercalates into the DNA double helix, and it will shift in a negative direction in the case of electrostatic interaction with DNA [56]. The observed shift toward more positive potentials reveals an interaction between the complexes and DNA and supports the results of the UV experiments, indicating an intercalative binding mode between the complexes and the DNA bases [57].

4. Conclusion

We have reported the synthesis of a pyrazolone derivative (H_2L) bearing a carbothioamide moiety using a heteropoly acid. This ligand has been characterized by IR, UV/visible, MS, ^1H and ^{13}C NMR spectrometry and electrochemistry. Its reactivity toward transition metal ions has been performed in solution with a potentiometric study that revealed complexation. Complexes of Cu(II) and Ni(II) have been prepared, characterized by IR, UV/visible, EPR, magnetic measurements, electrochemistry, and single-crystal X-ray diffraction. For each compound, the molecular structure consists of a discrete $[M(HL)_2(H_2O)]$ ($M = Cu^{II}$ (**A**) and Ni^{II} (**B**)) complex in which the metal ion has an $[M(SN)_2O]$ environment arising from two

chelating HL^- anionic ligands and a terminal water. In both cases, such coordination led to almost perfect trigonal bipyramidal geometries.

The observed electrochemical behavior of the complexes, in addition to the features of the ligand, which has a pyrazolone core known to be a bioactive heterocycle, display a potential antitumor profile. As a first step to get insight into the activity of the complexes, the interaction between the complexes and Fish-Sperm DNA has been studied by UV spectroscopy and electrochemistry, and revealed an intercalative mode. The binding strength has been assessed by UV titrations and revealed that **B** exhibited the higher binding constant. Previous studies reported that Ni(II) complexes could have better binding affinity than other metallic complexes. A review of the literature reveals that the planarity of the ligands and the presence of withdrawing elements in the ligand structures can enhance the binding strength. These elements are to be considered for the design of strong DNA-binding agents in the future.

As continuation of our work on bioactive complexes, docking studies and *in vitro* biological activities are conducted on a series of transition metal complexes including **A** and **B**.

Supplementary materials

Crystallographic data have been deposited in the Cambridge Crystallographic Data Center under the CCDC numbers CCDC 938436 (**A**) and 938,437 (**B**) that contains the supplementary crystallographic data for this paper. These data can be obtained free of charge via the web application at www.ccdc.cam.ac.uk/conts/retrieving.html [or from the Cambridge Crystallographic Data Center, 12 Union Road, Cambridge CB2 1EZ, UK; Fax: (internt.) + 44-1223-336-033; E-mail: deposit@ccdc.cam.ac.uk].

Acknowledgements

We gratefully acknowledge the Department of Inorganic Chemistry of the University Rey Juan Carlos (Spain) for the FS-DNA and the electrochemical measurements. We would like to thank Pr. Santiago Gomez for his advice and his help in the DNA-interaction study, and Pr. Isabel Del Hierro for her help in the electrochemical part of our work.

Disclosure statement

No potential conflict of interest was reported by the authors.

Funding

This work was supported by the CNRS (Centre National de la Recherche Scientifique); Brest University; French "Ministère de la Recherche and Ministère des Affaires Etrangères et Européennes"; PHC Maghreb [grant number 30255ZJ].

References

[1] A. Gursoy, S. Demirayak, G. Capan, K. Erol, K. Vural. *Eur. J. Med. Chem.*, **35**, 359 (2000).
[2] L.C. Behr, R. Fusco, C.H. Jarboe. In *The Chemistry of Heterocyclic Compounds, Pyrazoles, Pyrazolines, Pyrazolidines, Indazoles and Condensed Rings*, Interscience, New York (1967).

[3] S. Sugiura, S. Ohno, O. Ohtani, K. Izumi, T. Kitamikado, H. Asai, K. Kato. *J. Med. Chem.*, **20**, 80 (1977).
[4] G. Mariappan, B.P. Saha, L. Sutharson, A. Haldar. *Indian J. Chem.*, **49**, 1671 (2010).
[5] R.N. Mahajan, F.H. Havaldar, P.S. Fernandes. *J. Indian Chem. Soc.*, **68**, 245 (1991).
[6] N. Parekh, K. Maheria, P. Patel, M. Rathod. *Int. J. PharmTech. Res.*, **3**, 540 (2011).
[7] D. Bailey, P.E. Hansen, A.G. Hlavac, E.R. Baizman, J. Pearl, A.F. DeFelice, M.E. Feigenson. *J. Med. Chem.*, **28**, 256 (1985).
[8] F.A. Pasha, M. Muddassar, M.M. Neaz, S.J. Cho. *J. Mol. Graphics Modell.*, **28**, 54 (2009).
[9] E.S. Raper. *Coord. Chem. Rev.*, **129**, 91 (1994).
[10] M. Sobiesiak, I.P. Lorenz, P. Mayer, M. Wozniczka, A. Kufelnicki, U. Krajewska, M. Rozalski, E. Budzisz. *Eur. J. Med. Chem.*, **46**, 5917 (2011).
[11] E. Lakontseva, M. Krasavin. *Tetrahedron Lett.*, **51**, 4095 (2010).
[12] S.P. Maradur, G.S. Gokavi. *Catal. Commun.*, **8**, 279 (2007).
[13] Y. Guo, K. Li, X. Yu, J.H. Clark. *Appl. Catal., B Environ.*, **81**, 182 (2008).
[14] R. Fazaeli, S. Tangestaninejad, H. Aliyan, M. Moghadam. *Appl. Catal., A*, **309**, 44 (2006).
[15] R. Torviso, D. Mansilla, A. Belizán, E. Alesso, G. Moltrasio, P. Vázquez, L. Pizzio, M. Blanco, C. Cáceres. *Appl. Catal., A*, **339**, 53 (2008).
[16] S. Neidle, M. Waring (Eds.). *Molecular Aspects of Anticancer Drug-DNA Interactions*, Vol. 2, CRC Press, pp. 96–123, Taylor and Francis Group, London (1994).
[17] M. Hong, H. Geng, M. Niu, F. Wang, D. Li, J. Liu, H. Yin. *Eur. J. Med. Chem.*, **86**, 550 (2014).
[18] M.L. Glówka, M. Baszczyk, C.H. Prentjas, D. Kovala-Demertzi. *Pol. J. Chem.*, **78**, 2013 (2004).
[19] N. Lechani, M. Hamdi, F. Aklil, S. Khabouche, O. Benali Baitich, D. Kheffache, S. Moussi, O. Ouamerali. *Eur. J. Chem.*, **3**, 285 (2013).
[20] L.J. Bellamy, *The Infrared Spectra of Complex Molecules*, 2nd Edn, p. 355, Wiley, New York (1964).
[21] V.I. Vetrogon, N.G. Lukyanenko, M.J. Schwing-Weill, F. Arnaud-Neu. *Talanta*, **41**, 2105 (1994).
[22] S. Belaid, S. Djebbar, O. Benali Baitich, M.A. Khan, G. Bouet. *C.R. Chim.*, **10**, 568 (2007).
[23] CRYSALIS-CCD 170. Oxford-Diffraction, 2002. CRYSALIS-RED 170. Oxford Diffraction, Oxfordshire (2002).
[24] A. Altomare, M.C. Burla, G. Camalli, G. Cascarano, C. Giacovazzo, A. Gualiardi, G. Polidori. *J. Appl. Cryst.*, **27**, 435 (1994).
[25] G.M. Sheldrick. *SHELX97, Programs for Crystal Structure Analysis*. University of Göttingen, Göttingen, Germany (1997).
[26] L.J. Farrugia. *J. Appl. Crystallogr.*, **32**, 837 (1999).
[27] F. Dimiza, A.N. Papadopoulos, V. Tangoulis, V. Psycharis, C.P. Raptopoulou, D.P. Kessissoglou, G. Psomas. *J. Inorg. Biochem.*, **107**, 54 (2012).
[28] C. Protogeraki, E.G. Andreadou, F. Perdih, I. Turel, A.A. Pantazaki, G. Psomas. *Eur. J. Med. Chem.*, **86**, 189 (2013).
[29] (a) A.W. Addison, T.N. Rao, J. Reedijk, J. Van Rijn, G.C. Verschoor. *J. Chem. Soc., Dalton Trans.*, 1349 (1984); (b) M. Vaidyanathan, R. Balamurugan, U. Sivagnanam, M. Palaniandavar. *J. Chem. Soc., Dalton Trans.*, 3498 (2001).
[30] G. Foulds. *Coord. Chem. Rev.*, **80**, 1 (1987).
[31] E.S. Raper. *Coord. Chem. Rev.*, **129**, 91 (1994).
[32] B. Murphy, B. Hathaway. *Coord. Chem. Rev.*, **243**, 237 (2003).
[33] A.B.P. Lever. In *Inorganic Electronic Spectroscopy*, pp. 525–526, Elsevier, Amsterdam (1984).
[34] M. Ciampolini. *Inorg. Chem.*, **5**, 35 (1966).
[35] I. Bertini, M. Ciampolini, P. Dapporto, D. Gatteschi. *Inorg. Chem.*, **11**, 2254 (1972).
[36] B.J. Hathaway, D.E. Billing. *Coord. Chem. Rev.*, **5**, 143 (1970).
[37] D.L. Kepert. In *Inorganic Stereochemistry*, pp. 36–51, Springer, Berlin (1982).
[38] D. Reinen, M. Atanasov. *Chem. Phys.*, **136**, 27 (1989).
[39] M.A. Halcrow. *J. Chem. Soc., Dalton Trans.*, 4375 (2003).
[40] L. Husáriková, Z. Repická, J. Moncol, D. Valigura, M. Valko, M. Mazúr. *Appl. Magn. Reson.*, **44**, 571 (2013).
[41] M. Iqbal, S. Ali, Z.U. Rehman, N. Muhammad, M. Sohail, V. Pandarinathan. *J. Coord. Chem.*, **67**, 1731 (2014).
[42] R. Prabhakaran, R. Sivasamy, J. Angayarkanni, R. Huang, P. Kalaivani, R. Karvembu, F. Dallemer, K. Natarajan. *Inorg. Chim. Acta*, **374**, 647 (2011).
[43] K. Karami, M. Hosseini-Kharat, H. Sadeghi-Aliabadi, J. Lipkowski, M. Mirian. *Eur. J. Med. Chem.*, **73**, 8 (2014).
[44] R.R. Sinden. In *DNA Structure and Function*, p. 109, Academic Press, San Diego, CA (1994).
[45] A. Wolfe, G.H. Shimer Jr, T. Meehan. *Biochemistry*, **26**, 6392 (1987).
[46] Q.R. Cheng, F.Q. Zhang, H. Zhou, Z.Q. Pan, G.Y. Liao. *J. Coord. Chem.*, **68**, 1997 (2015).
[47] R.R. Duan, L. Wang, W.Q. Huo, S. Chen, X.H. Zhou. *J. Coord. Chem.*, **67**, 2765 (2014).
[48] M. Nandy, D.L. Hughes, G.M. Rosair, R.K. Singh, S. Mitra. *J. Coord. Chem.*, **67**, 3335 (2014).
[49] L. Subha, C. Balakrishnan, S. Thalamuthu, M.A. Neelakantan. *J. Coord. Chem.*, **68**, 1021 (2015).

[50] N. Shahabadi, M. Falsafi, S. Moradi Fili. *J. Coord. Chem.*, **68**, 1387 (2015).
[51] J. Lakshmipraba, S. Arunachalam, R. Vijay Solomon, P. Venuvanalingam. *J. Coord. Chem.*, **68**, 1374 (2015).
[52] P. Subbaraj, A. Ramu, N. Raman, J. Dharmaraja. *J. Coord. Chem.*, **67**, 2747 (2014).
[53] A. Qasem Ali, S. Guan Teoh, N. Eltaher Eltayeb, M.B. Khadeer Ahamed, A. Abdul Majid. *J. Coord. Chem.*, **67**, 3380 (2014).
[54] H. Wu, X. Wang, Y. Zhang, F. Shi, Y. Bai, H. Wang, G. Pan. *J. Coord. Chem.*, **67**, 660 (2014).
[55] G. Psomas. *J. Inorg. Biochem.*, **102**, 1798 (2008).
[56] F. Dimiza, A.N. Papadopoulos, V. Tangoulis, V. Psycharis, C.P. Raptopoulou, D.P. Kessissoglou, G. Psomas. *Dalton Trans.*, **39**, 4517 (2010).
[57] M. Zampakou, M. Akrivou, E.G. Andreadou, C.P. Raptopoulou, V. Psycharis, A.A. Pantazaki, G. Psomas. *J. Inorg. Biochem.*, **121**, 88 (2013).